Solid Earth

Supporting Information for

Seismic source characterization from GNSS data using deep learning

Giuseppe Costantino[1], Sophie Giffard-Roisin[1],

David Marsan[1], Mathilde Radiguet[1], Mauro Dalla Mura[2, 3], Anne Socquet[1]

[1]Univ. Grenoble Alpes, Univ. Savoie Mont Blanc, CNRS, IRD, Univ. Gustave Eiffel, ISTerre, 38000 Grenoble, France

[2]Univ. Grenoble Alpes, CNRS, Grenoble INP, GIPSA-lab, 38000 Grenoble, France

[3]Institut Universitaire de France (IUF), France

Contents of this file

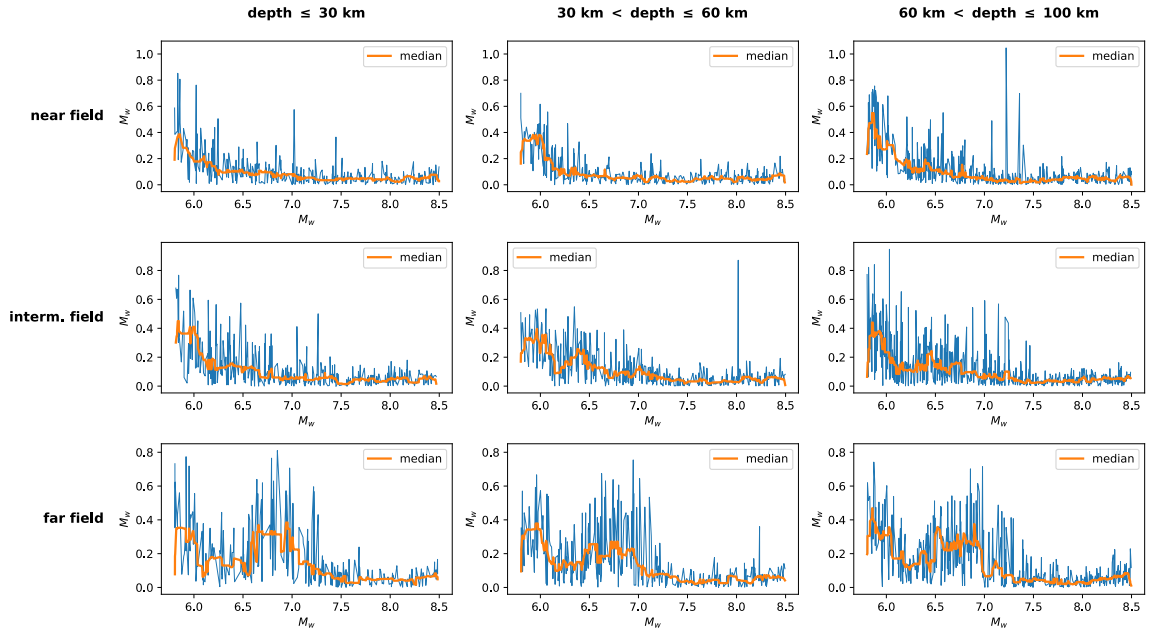

Figure S1. Magnitude error, computed for each test sample, as a function of the magnitude (x axis), the depth range (columns) and the distance range (cf. fig. 6) with respect to the GNSS network (rows) for TRA. The orange solid line represents the result of a median smoothing by employing a kernel size of 15 points.

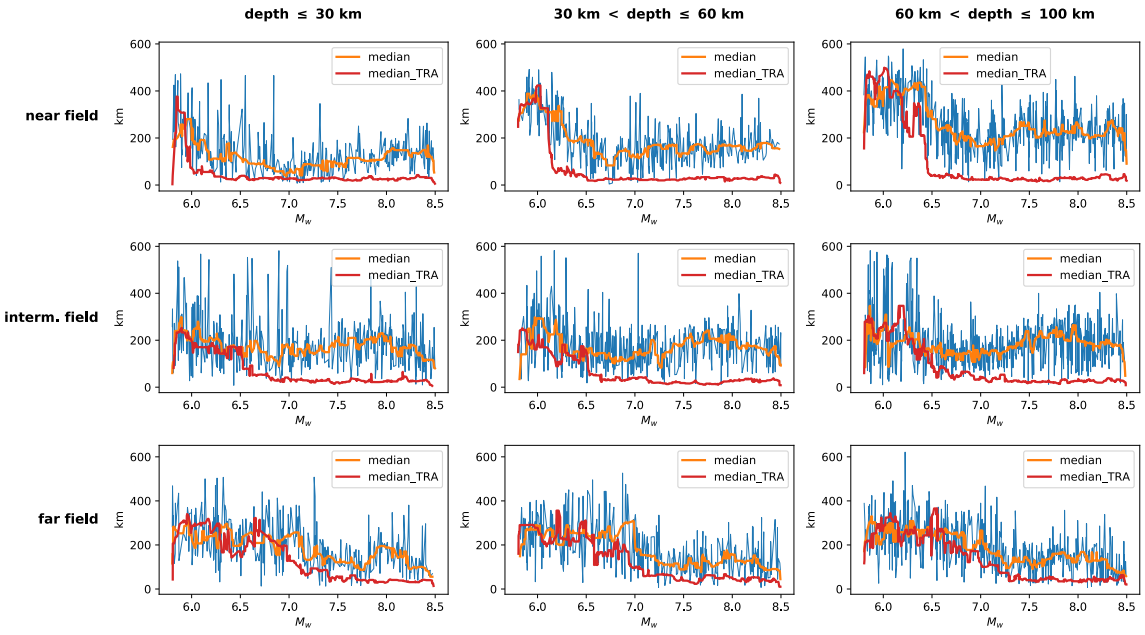

Figure S2. Position error, computed for each test sample, as a function of the magnitude (x axis), the depth range (columns) and the distance range (cf. fig. 6) with respect to the GNSS network (rows) for TS. The orange solid line represents the result of a median smoothing by employing a kernel size of 15 points. The red solid line represents the TRA median (cf. fig. 7).

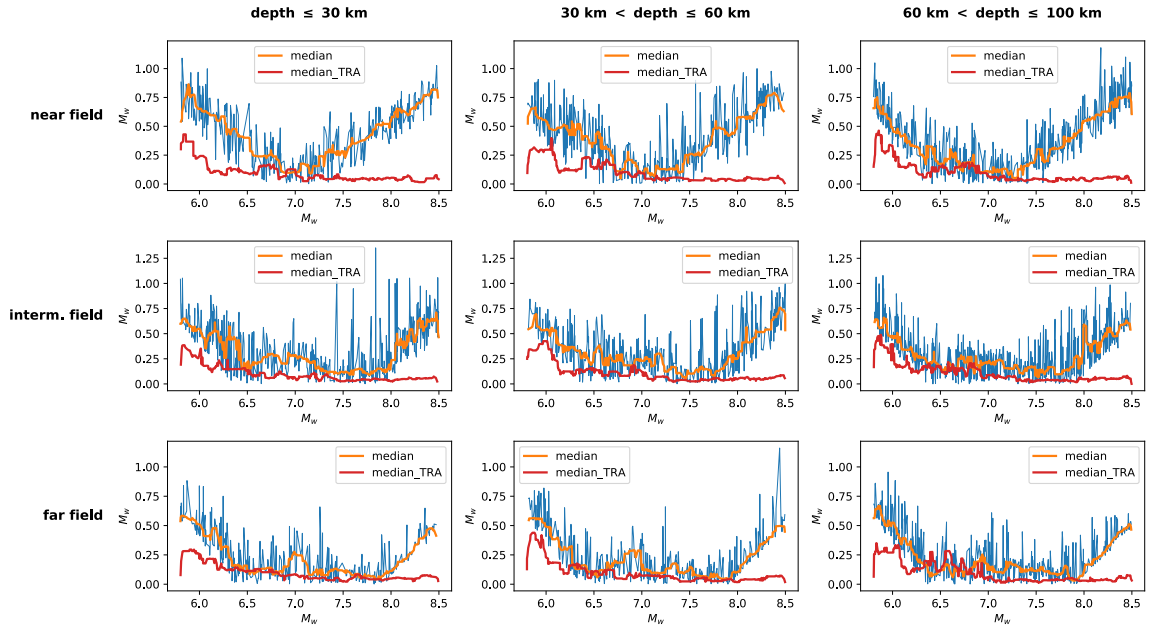

Figure S3. Magnitude error, computed for each test sample, as a function of the magnitude (x axis), the depth range (columns) and the distance range (cf. fig. 6) with respect to the GNSS network (rows) for TS. The orange solid line represents the result of a median smoothing by employing a kernel size of 15 points. The red solid line represents the TRA median (cf. fig. S1).

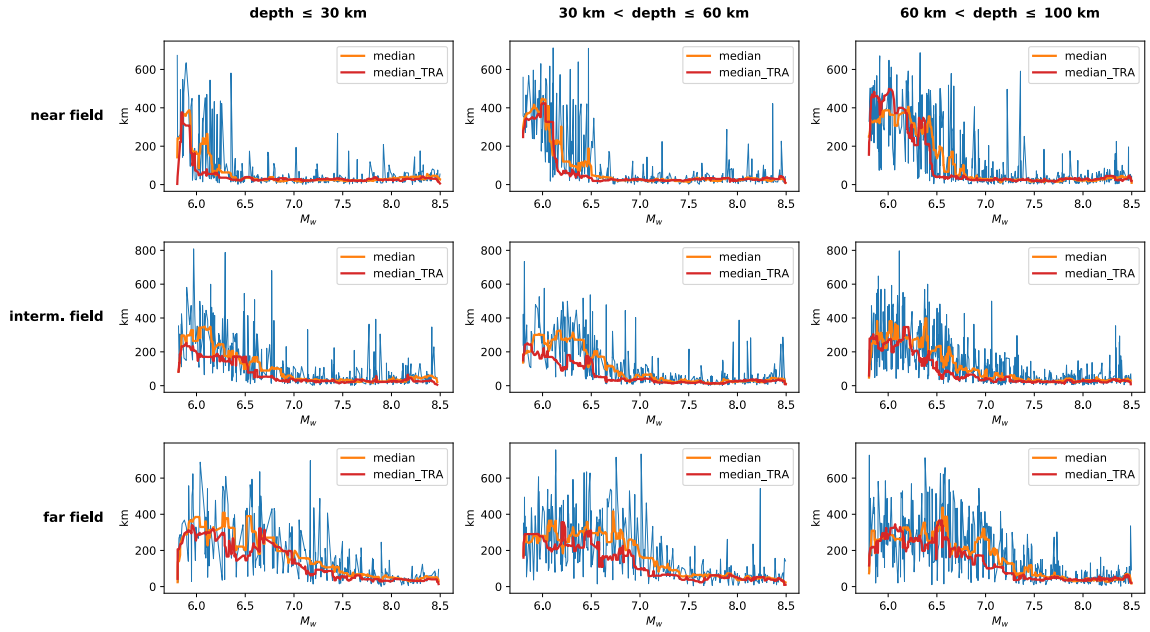

Figure S4. Position error, computed for each test sample, as a function of the magnitude (x axis), the depth range (columns) and the distance range (cf. fig. 6) with respect to the GNSS network (rows) for IMG. The orange solid line represents the result of a median smoothing by employing a kernel size of 15 points. The red solid line represents the TRA median (cf. fig. 7).

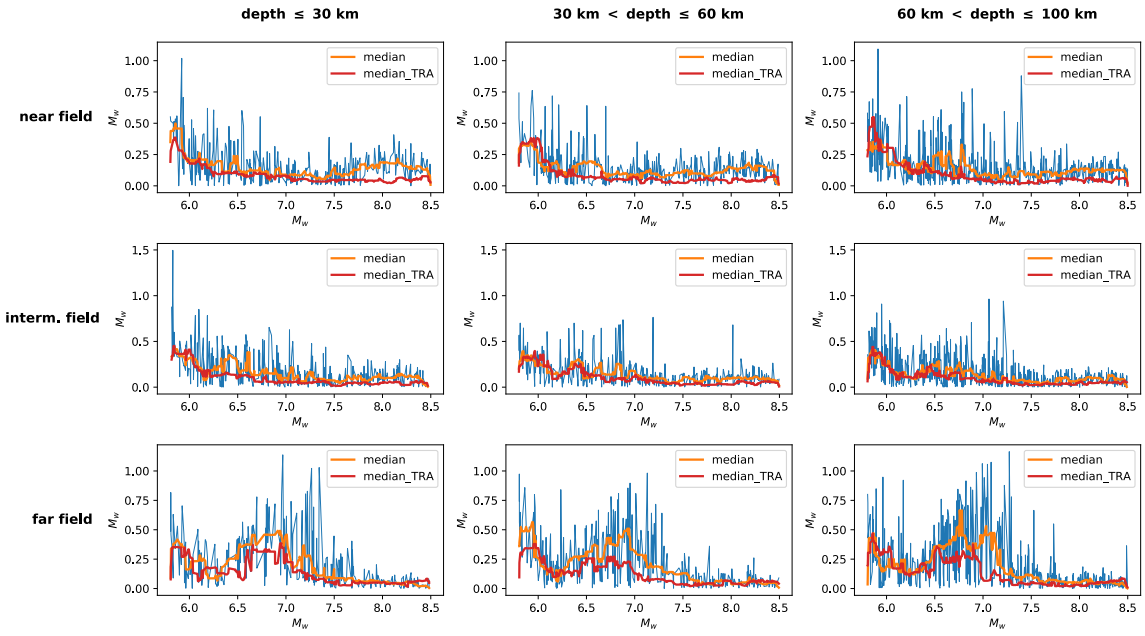

Figure S5. Magnitude error, computed for each test sample, as a function of the magnitude (x axis), the depth range (columns) and the distance range (cf. fig. 6) with respect to the GNSS network (rows) for IMG. The orange solid line represents the result of a median smoothing by employing a kernel size of 15 points. The red solid line represents the TRA median (cf. fig. S1).

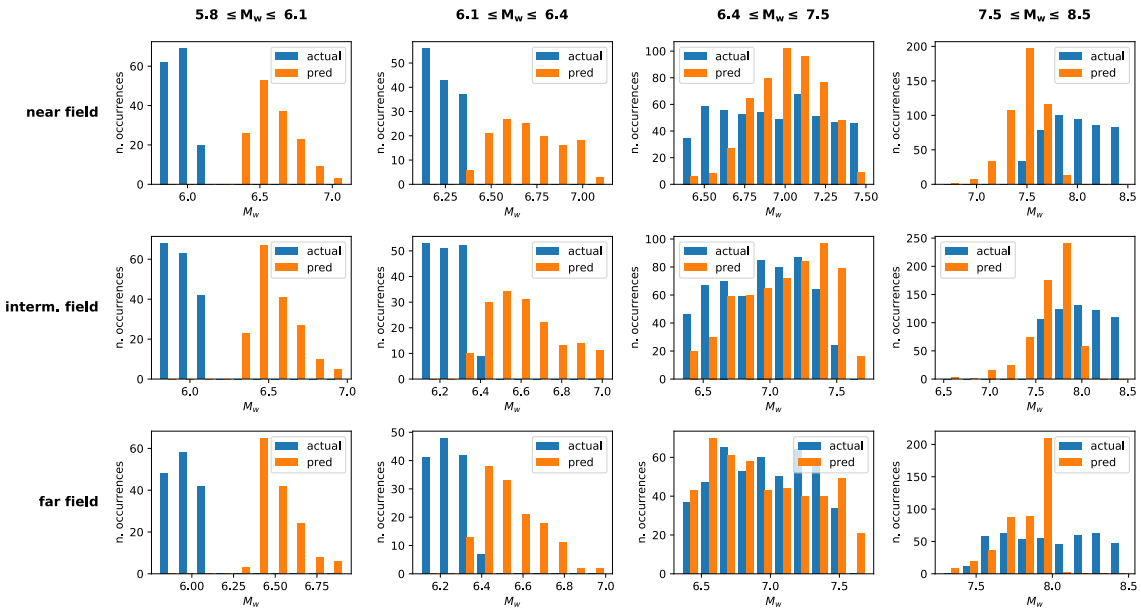

Figure S6. Histograms of the predicted magnitude (orange bars) with respect to actual (test) magnitude (blue bars) as a function of the distance range (cf. fig. 6) with respect to the GNSS network (rows) and for different magnitude ranges (columns), for TS.

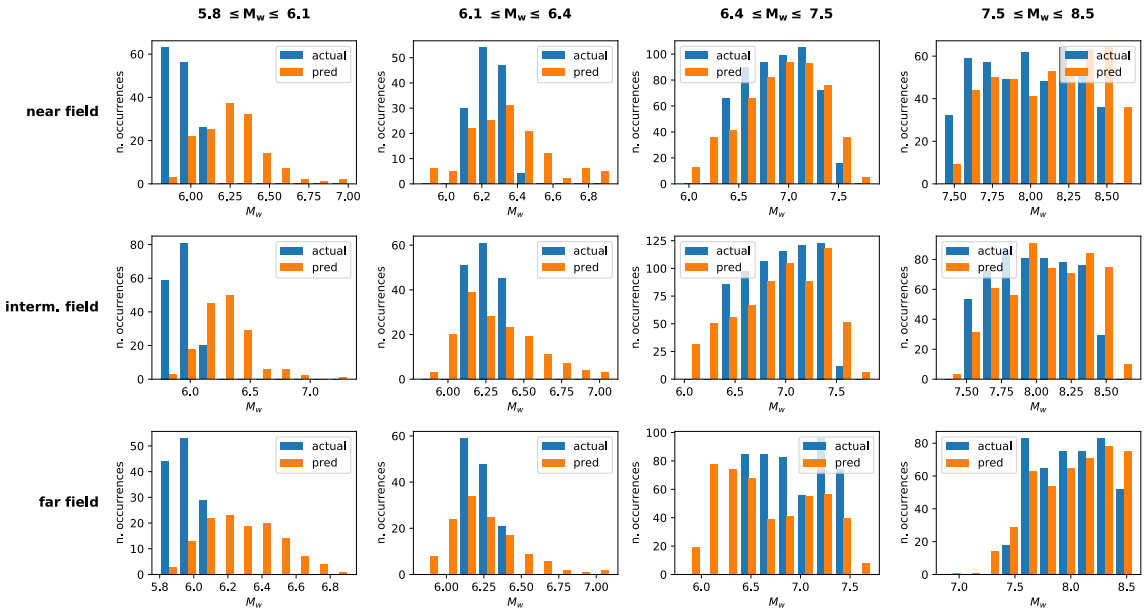

Figure S7. Histograms of the predicted magnitude (orange bars) with respect to actual (test) magnitude (blue bars) as a function of the distance range (cf. fig. 6) with respect to the GNSS network (rows) and for different magnitude ranges (columns), for IMG.

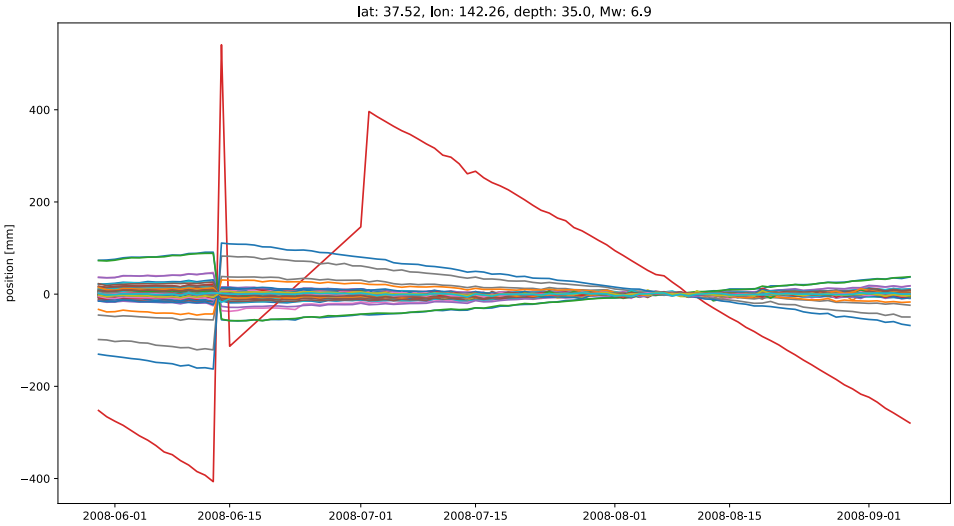

Figure S8. Interpolated time series (N-S component) associated to a 100—day window centered onto the 19 July 2008 for the **GAMIT** data set. Each line represents a different GEONET station. The red line is an artifact caused by a large data gap, producing a false westwards displacement, which hides the eastwards displacement due to the seismic signal.

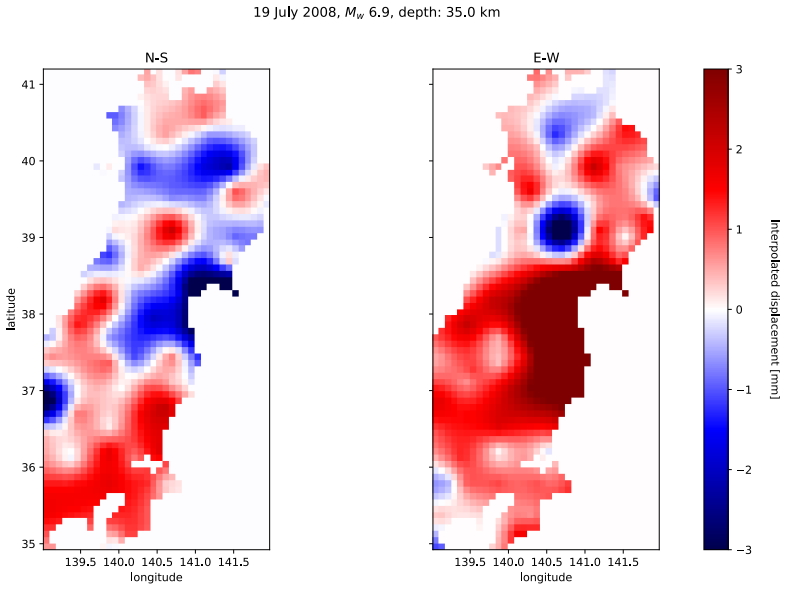

Figure S9. Differential image (N-S component) associated to the 19 July 2008 for the **GAMIT** data set. The deformation value has been saturated over $\pm$3 mm.

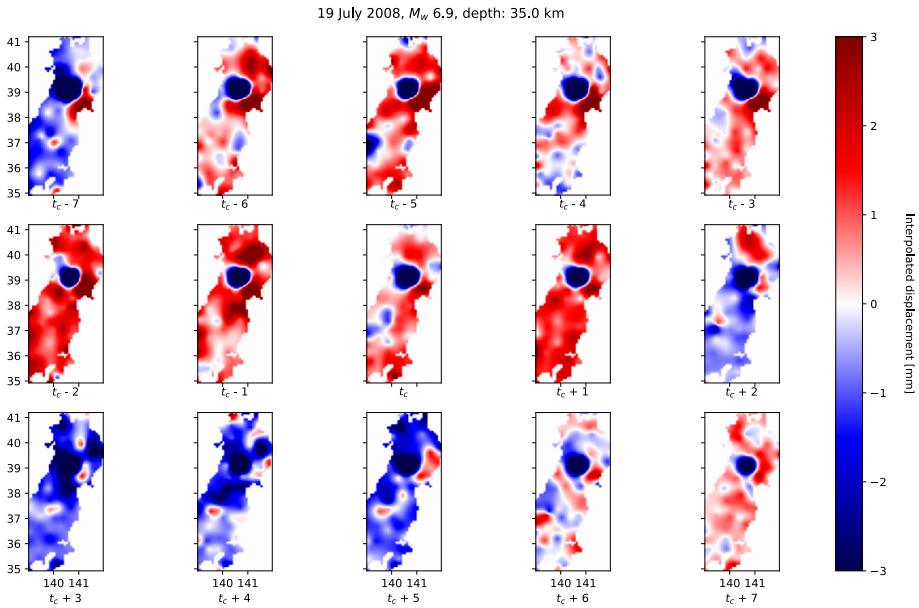

Figure S10. Image time series (N-S component) associated to the 19 July 2008 for the **GAMIT** data set. The deformation value has been saturated over ± 3 mm. Each frame is associated to the day written below (*e.g.*, $\boldsymbol{t_c - 2}$, where $\boldsymbol{t_c}$ is the time associated to the coseismic offset).

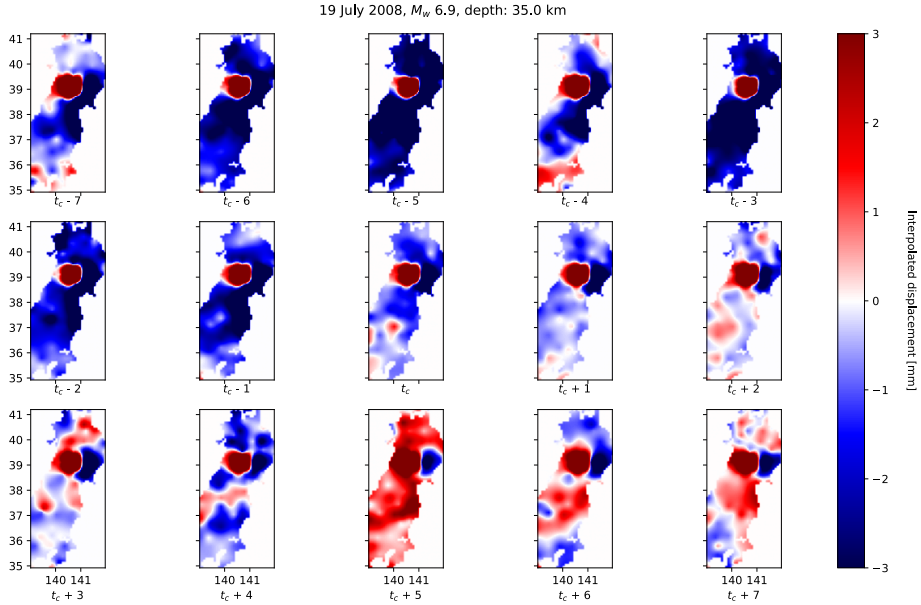

Figure S11. Image time series (E-W component) associated to the 19 July 2008 for the **GAMIT** data set. The deformation value has been saturated over ± 3 mm. Each frame is associated to the day written below (*e.g.*, $\boldsymbol{t_c - 2}$, where $\boldsymbol{t_c}$ is the time associated to the coseismic offset).

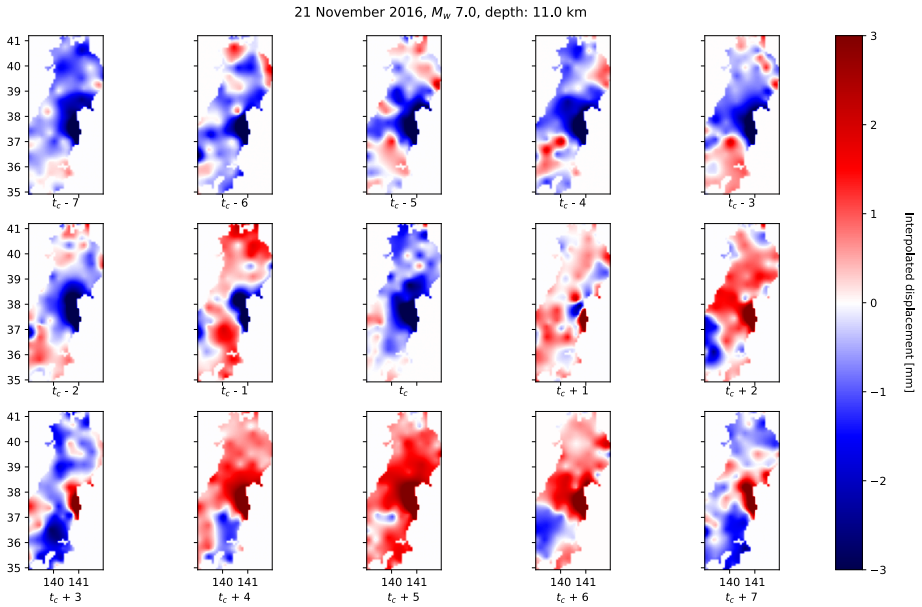

Figure S12. Image time series (N-S component) associated to the 21 November 2016 for the **GAMIT** data set. The deformation value has been saturated over $\pm$3 mm. Each frame is associated to the day written below (*e.g.*, $\boldsymbol{t_c - 2}$, where $\boldsymbol{t_c}$ is the time associated to the coseismic offset).

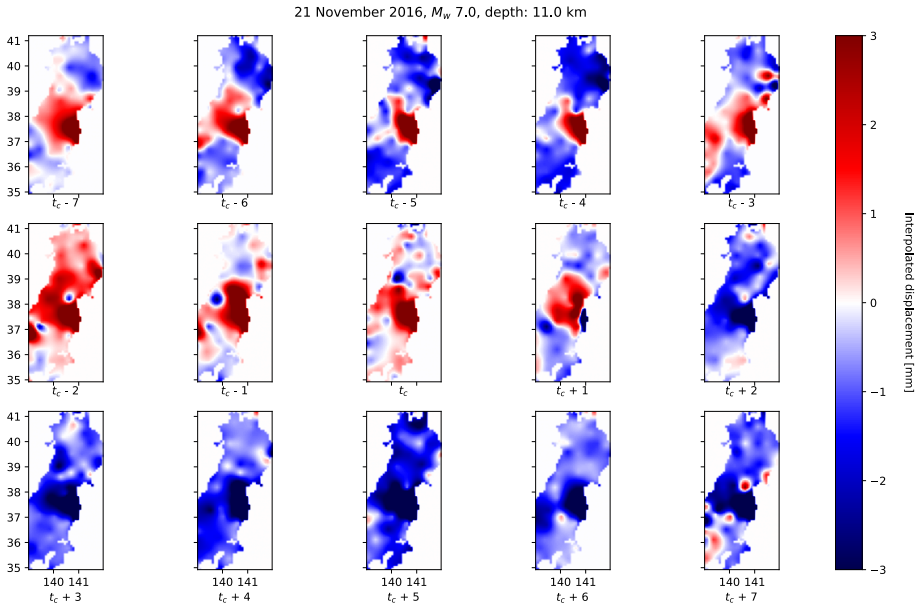

Figure S13. Image time series (E-W component) associated to the 21 November 2016 for the **GAMIT** data set. The deformation value has been saturated over $\pm$3 mm. Each frame is associated to the day written below (*e.g.*, $\boldsymbol{t_c - 2}$, where $\boldsymbol{t_c}$ is the time associated to the coseismic offset).

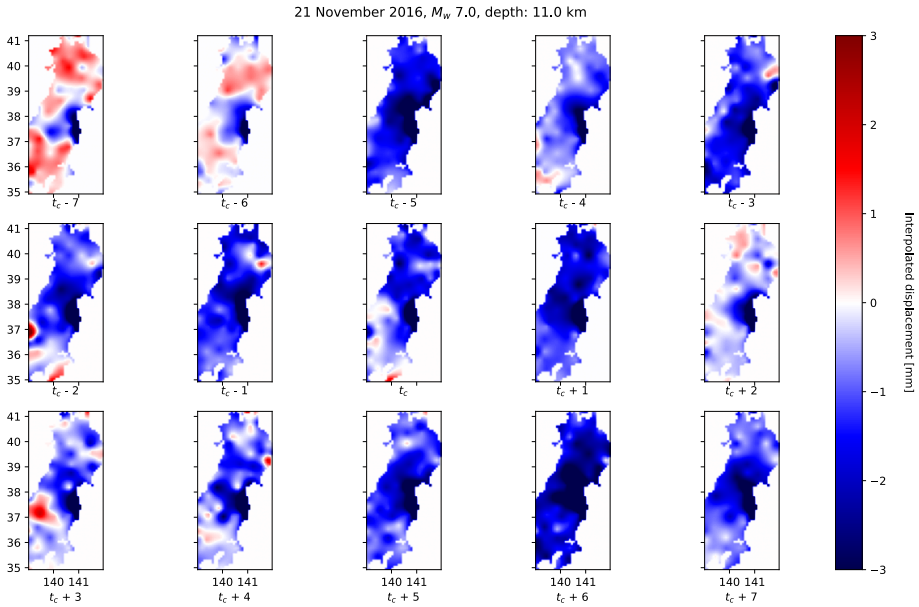

Figure S14. Image time series (N-S component) associated to the 21 November 2016 for the **NGL** data set. The deformation value has been saturated over ± 3 mm. Each frame is associated to the day written below (*e.g.*, $\boldsymbol{t_c - 2}$, where $\boldsymbol{t_c}$ is the time associated to the coseismic offset).

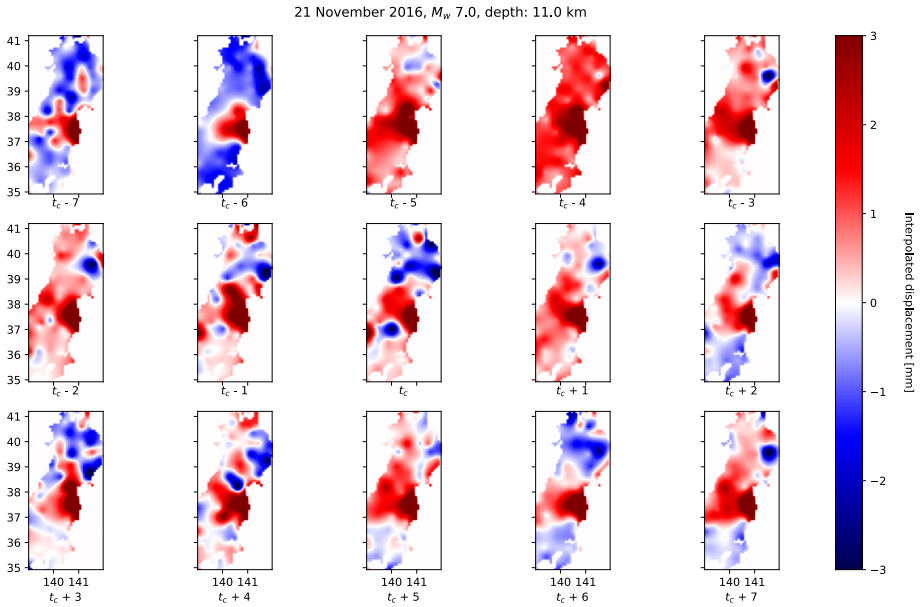

Figure S15. Image time series (E-W component) associated to the 21 November 2016 for the **NGL** data set. The deformation value has been saturated over ± 3 mm. Each frame is associated to the day written below (*e.g.*, $\boldsymbol{t_c - 2}$, where $\boldsymbol{t_c}$ is the time associated to the coseismic offset).

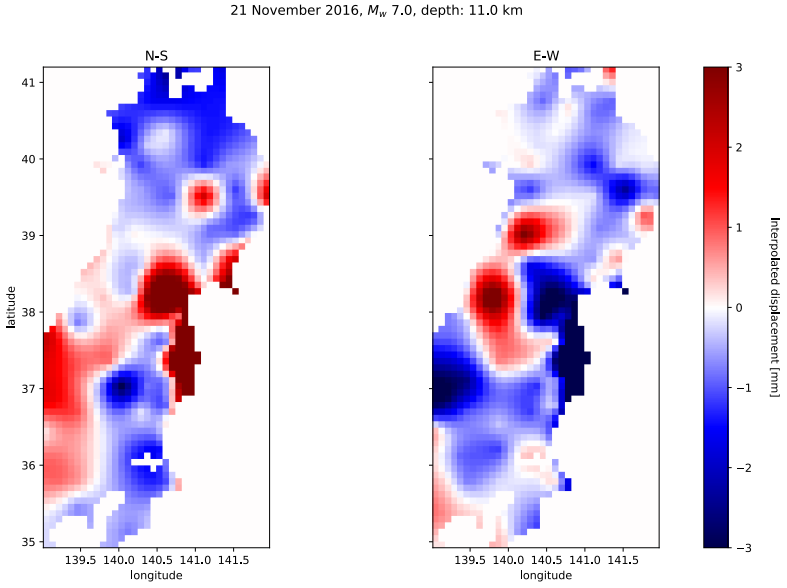

Figure S16. Differential image associated to the 21 November 2016 for the **GAMIT** data set. The deformation value has been saturated over ± 3 mm.

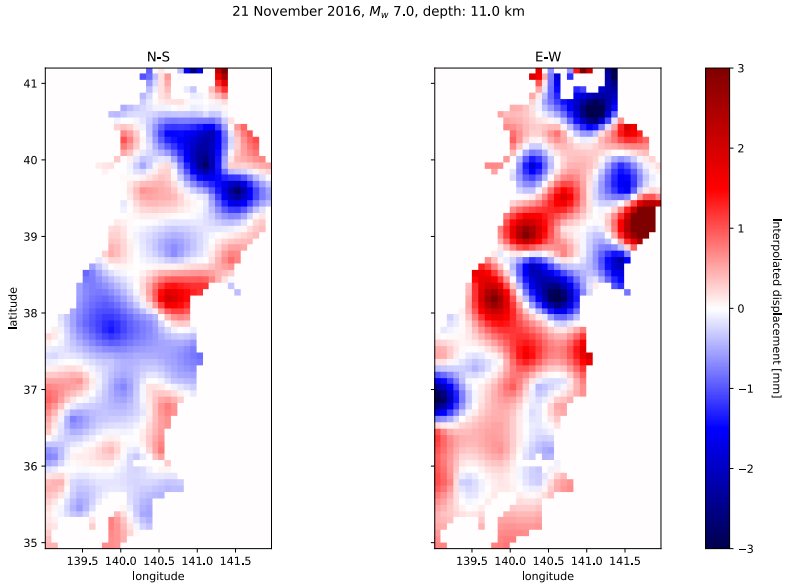

Figure S17. Differential image associated to the 21 November 2016 for the **NGL** data set. The deformation value has been saturated over ±3 mm.